Solar Energy 225 (2021) 399–406

Contents lists available at ScienceDirect

Solar Energy

journal homepage: www.elsevier.com/locate/solener

Synthesis of a carboxylic acid-based ruthenium sensitizer and its applicability towards Dye-Sensitized Solar Cells

Arumugam Pirashanthan [a,b], Murugathas Thanihaichelvan [a], Kadarkaraisamy Mariappan [c], Dhayalan Velauthapillai [b,*], Punniamoorthy Ravirajan [a], Yohi Shivatharsiny [d,*]

[a] Clean Energy Research Laboratory, Department of Physics, University of Jaffna, Jaffna 40000, Sri Lanka
[b] Faculty of Engineering and Science, Western Norway University of Applied Sciences, 5020 Bergen, Norway
[c] Department of Chemistry, University of South Dakota, Vermillion, SD 57069, USA
[d] Department of Chemistry, University of Jaffna, Jaffna 40000, Sri Lanka

ARTICLE INFO

Keywords:
Ruthenium dye
Titanium dioxide
Solar cells
Mass spectrum
Cyclic voltammetry
External quantum efficiency

ABSTRACT

This work reports the synthesis of ruthenium based $Ru(bpy)_2(dcbpy)(ClO_4)_2$[(bpy)2,2′-bipyridine;dcbpy = 4,4′-dicarboxy-2,2′-bipyridine] (RuC) dye and its application in solid and liquid state Dye-Sensitized Solar Cells (DSSCs). Synthesis resulted with high-pure orange coloured dye with a high yield percentage of 45%. The dye was characterized *via* Nuclear Magnetic Resonance (NMR) spectroscopy, Mass spectroscopy, Cyclic Voltammetry (CV) and UV–vis spectroscopy. The calculated bandgap (E_g) of 2.38 eV from absorbance spectra of pure RuC in ethanol solution showed best proximity with the data obtained from CV measurements. The RuC showed strong absorption in near UV region with the highest molar extinction coefficient (MEC) of 14,746 $M^{-1}cm^{-1}$ at 463 nm. Plateau of over 80% of External Quantum Efficiency (EQE) spectra reveals the efficient carrier generation of RuC in near UV region. Carboxylic acid groups of RuC provide the potential for enhanced electron transfer from TiO_2 surface, and an increased electron density at the interface leads to higher current density. The RuC sensitized solid and liquid state DSSCs exhibited a short circuit current density (J_{SC}) over 3.04 mA/cm^2 and 5.82 mA/cm^2, and power conversion efficiency (PCE) of 1.2% and 1.8% respectively under simulated Air Mass 1.5 irradiation (100 $mWcm^{-2}$).

1. Introduction

The Dye-Sensitized Solar Cells (DSSCs) have emerged as a promising economical photovoltaic device due to its flexibility, light weight, ease of fabrication, transparency, high power conversion efficiencies in diffuse light conditions, facile synthesis, eco-friendly nature etc. (Omar et al., 2020). The concept of DSSC was first introduced by Tennakone et al in 1988 [3], and O'Regen and Grätzel reported an efficiency of 7.1% in 1991 (Lee et al., 2017; O'Regan and Grätzel, 1991). Since then hundreds of studies are carried out to enhance the performance of DSSCs, and the reported record efficiency is around 14% [2]. To make DSSC a competitive PV technology in the market, a variety of issues that challenges DSSCs had to be sorted out. Research community has been focusing on improving their stability, durability, efficiency and reducing the cost of production (Mariotti et al., 2020). The major drawback with DSSC is the use of liquid electrolytes, which cause temperature stability issues. Electrolyte is crucial in DSSC for the inner charge carrier transportation between electrodes and continuous regeneration of the dye during the DSSC operation (Wu et al., 2015). Further, the interface between the electrolyte and electrodes significantly influences charge transport across the fabricated solar cell. Therefore, the choice of electrolyte is a focused issue, and intensive research has been carried out on liquid state, quasi-solid state, and solid-state electrolytes for DSSCs. (Chen et al., 2011; Dissanayake et al., 2021; Karakuş et al., 2020; Lee and Ho, 2018; Mehmood et al., 2017). The solid electrolyte based DSSCs have shown to have good mechanical stability and simpler fabrication techniques compared to liquid electrolyte based DSSCs (Zhang et al., 2018).

Titanium dioxide is a widely used material in both solid and liquid state solar cells as well as in various applications, such as solar energy utilization for hydrogen production through water splitting (Mahoney et al., 2015b; Shanmugaratnam et al., 2019), environmental

* Corresponding authors.
E-mail addresses: pirashanthan.arumugam@gmail.com (A. Pirashanthan), thanihai@gmail.com (M. Thanihaichelvan), Kadarkaraisamy.Mariappan@usd.edu (K. Mariappan), Dhayalan.Velauthapillai@hvl.no (D. Velauthapillai), pravirajan@univ.jfn.ac.lk (P. Ravirajan), yshiva@univ.jfn.ac.lk (Y. Shivatharsiny).

https://doi.org/10.1016/j.solener.2021.07.056
Received 17 March 2021; Received in revised form 11 July 2021; Accepted 22 July 2021
Available online 27 July 2021

remediation applications (Senthilnanthan et al., 2010), and electrochromic applications(Abate et al., 2014; Dissanayake et al., 2019; Mahoney et al., 2015a; Maleki et al., 2021; Rasalingam et al., 2015a; Ravirajan et al., 2012). Among the Titanium dioxide polymorphs, the anatase TiO_2 is widely used in photovoltaic applications due to its higher activity with good chemical stability, and can be prepared in different forms and sizes with highly ordered porosity and crystallinity (Deiana et al., 2016, 2013; Patrocinio et al., 2015). Further, several dyes had been used as a sensitizer in Titanium dioxide-based photovoltaics. The combined use of organic small molecules and inorganic semiconductor materials facilitate energy level tuning via varying the chemical structure (Fournier et al., 2018). Particularly the metal complexes such as ruthenium (Ru(II)) (Aguirre-Araque et al., 2020; Chang et al., 2012; Swarnalatha et al., 2016), containing organic ligands functionalized with carboxylic substituents as anchoring groups to the TiO_2 have intensively been investigated for DSSC application because of their broad absorption spectra and favorable photovoltaic properties (Baktash et al., 2016; Gorduk and Altindal, 2019; Sodeyama et al., 2012; Song et al., 2009; Tsaturyan et al., 2018; Veronese et al., 2019). It was found that the surface binding on TiO_2 metal oxide and the performance of fabricated solar cells were strongly influenced by both the chemical structure and the number of anchoring groups (Abdellah et al., 2019; Abdellah and El-Shafei, 2020; Park et al., 2006). In this regard, the carboxylic acid (–COOH) is an effective anchoring group compared to other anchoring groups like phosphonate and acetylacenonate in order to bind well with the TiO_2 which results these dyes having good adsorption on the TiO_2 surface (Braumüller et al., 2016; El Bitar Nehme et al., 2019; Giribabu et al., 2011; Neuthe et al., 2014; Park et al., 2006). In this case, the interaction between the dye and TiO_2 metal oxide is improved by involves either rapid proton shuttling between a carboxylic acid and the surface oxygen, or proton sharing due to quantum delocalization (Tabacchi et al., 2019). Furthermore, a crucial light absorption in the visible region is observed from the solar spectrum, due to the high charge transfer by metal complex (Pirashanthan et al., 2020). A broad absorption spectrum, suitable excited and ground state energy levels, relatively long excited-state lifetime and good electrochemical stability of Ru complexes resulted in the best photovoltaic performance in DSSCs (Oh et al., 2018). In addition, ruthenium is the most suitable element with a good band edge position, thus most of the dyes used in the recent era for photovoltaic devices are ruthenium based. For example, N719, N3 and Z907 dyes are the commercially available dyes for DSSC applications; the major difference between these dyes is the placement of ruthenium (Ru) in their organic structure (Chang et al., 2012; Khan et al., 2017; Sugathan et al., 2015; Wu et al., 2017). Since, these commercial products are comparatively expensive, in this work a novel ruthenium based $Ru(bpy)_2(dcbpy)(ClO_4)_2$[(bpy)2,2′-bipyridine; dcbpy = 4,4′-dicarboxy-2,2′-bipyridine](RuC) dye was synthesized with a better anchoring group (–COOH) and RuC is used as a sensitizer to enhance the performance of solid and liquid state DSSCs.

The better compatibility of the energy levels of lowest unoccupied molecular orbital (LUMO) of the sensitizers and the band edge of the semiconductor metal oxide are important key factors to influence the electron injection of ruthenium sensitizers based solar cells (Aguirre-Araque et al., 2020; Louazri et al., 2016; Veronese et al., 2019). Carboxylic acid groups of RuC provide an enhanced electron transfer from the TiO_2 surface and thus increase electron density at the interface that leads to higher current density. Here we report the synthesis and characterization of a novel, cost effective ruthenium based $Ru(bpy)_2(dcbpy)(ClO_4)_2$[(bpy)2,2′-bipyridine;dcbpy = 4,4′-dicarboxy-2,2′-bipyridine](RuC) dye and its applicability towards solid-state and liquid-state DSSCs. Notably, few research articles can be found on synthesized Ru based dyes for DSSC application, however these lack detailed analysis of the dye and its characterization. This paper provides new insight in to cost effective synthesized ruthenium based dye for DSSC application.

2. Materials and methods

2.1. Synthesis of RuC

All reagents, lithium perchlorate ($LiClO_4$), 2,2′-Bipyridine-4,4′-dicarboxylic acid (dcbpy), *cis*-Bis(2,2′-bipyridine)dichlororuthenium(II) hydrate($Ru(bpy)_2Cl_2$), Methanol (CH_3OH) were used without further purification. Deionized (DI) water was used as diluent. Appropriate amounts of *cis*-Bis(2,2′-bipyridine)dichlororuthenium(II) hydrate($Ru(bpy)_2Cl_2$) (0.5 g, 1.0 mmol), 2,2′-bipyridine-4,4′-dicarboxylic acid (dcbpy) (0.3 g, 1.2 mmol) and sodium bicarbonate (0.3 g, 3.6 mmol) were mixed in basic media using methanol : water (v/v = 1:1.5) as solvent. This mixture was then refluxed for 2 h under Argon atmosphere. Then, the crystals were solidified by adding saturated aqueous lithium perchlorate in acidic medium and allowed for over-night refrigeration (Rasalingam et al., 2015b). A Red orange solid was obtained when the solution's pH was brought into acidic by using 70% $HClO_4$. Solid was then filtered and air-dried. The entire solid was dissolved in dry acetonitrile and diethyl ether was diffused into it.

2.2. Dye material characterization

UV–vis measurement of the dye molecules was recorded by using a Cary 100 Bio UV–vis spectrophotometer. A Varian 500-MS Ion Trap Mass Spectrometer was used for mass identification. Cyclic Voltammetry (CV) of RuC was recorded using a CH instruments 660 electrochemical workstation. 0.1 M tetrabutylammonium perchlorate solution with CH_3CN was used as a solvent against Ag/AgCl as the reference electrode. The CV measurement was done with 1 mM RuC in acetonitrile at room temperature under an inert atmosphere.

2.3. Solar cell fabrication

The device structure of fabricated RuC sensitized solid-state and liquid-state DSSCs are shown in Fig. 1. Cleaned Indium Tin Oxide (ITO) coated glass substrates with the area of 1 cm^2 were used to fabricate the solid-state solar cells. The ITO substrates were first coated by aerosol spray pyrolysis deposition of TiO_2 precursor at 500 °C in order to form ~50 nm thick compact TiO_2 layer as described in ref (Pirashanthan et al., 2020, 2019; Prashanthan et al., 2017). Mesoporous TiO_2 layer was then spin-coated on the top of the compact TiO_2 with the solution of TiO_2 paste (Dyesol 18NRT) dissolved in tetrahydrofuran (240 mg/mL). The TiO_2 films were slowly heated and allowed to sinter at 450 °C for 30 min. Once cooled, the mesoporous TiO_2 layers were immersed into 0.3 mM concentrated RuC dye solution in order to improve the spectral response. The dye solution was prepared using the 1:1 solvent mixture of acetonitrile and *tert*-butanol. Excess dye was removed by rinsing the films with the same solvent mixture. The RuC sensitized TiO_2 mesoporous films were used to prepare solid-state DSSCs with spiro-OMeTAD as hole transporter as shown in Fig. 1**(a)**. For the Spiro deposition, 97 mg/mL solution of Spiro-OMeTAD in chlorobenzene (A), 175 mg/mL solution of bis(trifluoromethane)sulfonimide lithium salt in Acetonitrile (B), and 46.6% (v/v) solution of 4-*tert*-butylpyridine (TBP) in Acetonitrile (C) were prepared separately. Then, 1200 μL of solution A, 36.24 μL of solution B and 11.7 μL of solution C, were taken and allowed to mix well for 40 min. Once the clear solution was observed, it was dispensed on the substrate and allowed to spread across the area of the substrate through spin coating. Finally, the solid-state devices were coated with thermally evaporated 100 nm thick gold (Au) electrode under high vacuum. After deposition, the substrates were sintered under a nitrogen medium.

The DSSCs with liquid Iodine (I^-/I^{3-}) electrolyte as shown in Fig. 1 **(b)** were fabricated using TiO_2 coated TEC15 FTO glass electrode which was purchased from Dyesol (TiO_2 coated transparent test cell glass electrodes, consists a layer of transparent nanocrystalline with an average grain size of 20 nm and a TiO_2 layer with a thickness of 12 (±1)

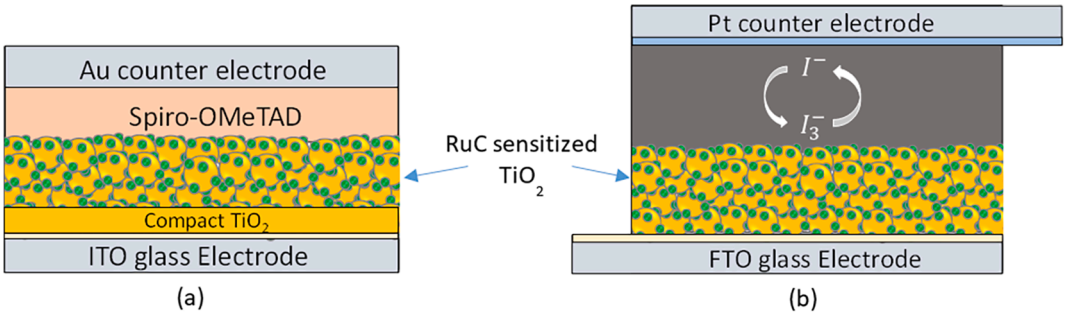

Fig. 1. The device structure of fabricated RuC sensitized **(a)** solid-state and **(b)** liquid-state DSSCs.

μm). These electrodes were dipped into the 0.3 mM dye solution overnight. The platinum counter electrode and the iodide electrolyte were also purchased from Dyesol.

2.4. Solar cell characterization

UV–Vis measurement of the dye sensitized mesoporous TiO_2 thin films were recorded by using JENWAY 6800 UV/Vis Spectrophotometer with Flight Deck software. The current density *vs.* voltage measurement of fabricated solar cells was tested and recorded with SCIENCE TECH solar simulator and computer controlled Keithley 2400 source meter. Both solid-state and liquid-state DSSCs were tested under conditions of dark and 100 mW/cm^2 (1 sun) illuminations with 1.5 Air Mass spectral filter. The External Quantum Efficiency measurements were done by using a standard Silicon UV enhanced photodiode, monochromator, and Keithley 2400 source meter.

3. Results and discussion

3.1. Synthesis of RuC

A crystalline solid with a yield percentage of 45% was attained with high purity, and the melting point of the as-prepared crystals was found to be $> 300^{\circ}$C. The chemical structure and optical photograph of synthesized RuC dye are shown in Fig. 2.

Fig. 3**(a)** illustrates the absorbance and emission spectra of 0.05 mM solution (in ethanol) of RuC dye recorded using the UV–Visible spectrometer. The absorption spectra showed strong absorption in the near UV region with a sharp decay tailing around 500 nm and, absorbance and emission lines intersect at the wavelength of approximately 560 nm. The optical bandgap energy was found to be ~ 2.39 eV through the wavelength at the saturation point (λ_{onset}) of absorbance spectrum as shown in Fig. 3**(b)**.

The formation of RuC dye molecule is further evidenced by the mass spectrum of pure RuC, which is shown in Fig. 4. The peak at *m/z* value of 658 revealed the formation of the M^{2+} ion species of RuC dye molecule and the peak at *m/z* value of 329.4 is due to the autoionization of the dye molecule.

Fig. 5 represents the Nuclear Magnetic Resonance Spectroscopic (NMR) interpretation of synthesized RuC dye. Hydrogen (^{1}H) and Carbon (^{13}C) NMR were taken to the dye molecule in CD_3CN solvent at 25 °C, and the figures are given in the supporting information section (Figs. S1 and S2). The multiplet splitting pattern attained at chemical shift ranges of 7.38–7.49, and 7.66–7.71 ppm is due to the four aromatic hydrogen (m, 4H, Ar-H_f and m, 4H, ArH_g), respectively. Other multiplets obtained at 7.81–7.83 (m, 2H, Ar-H_c); 7.93–7.95 (m, 2H, ArH_b); 8.05–8.11 (m, 4H, Ar-H_e); and 8.51–8.54 (m, 4H, Ar-H_h); and doublets obtained at 8.55–8.65 ppm (d, 2H, Ar-H_d) is due to aromatic hydrogens as indicated by the respective numbers. A singlet obtained at 9.02 (s, 2H, Ar-H_a) is due to the hydrogen from dcbpy. The carbon NMR shits obtained at 124.9; 125.4; 125.5; 127.8; 128.7; 128.8; 139.3; 139.8; 152.6; 152.8; 153.8; 157.6; 157.8; 158.7 and 165.1 ppm further confirm the purity of RuC dye.

CV measurements carried out in a 0.1 M tetrabutylammonium perchlorate solution with CH_3CN as solvent against Ag/AgCl as the reference electrode is shown in Fig. 6. The band positions of the dye material were obtained by finding its' highest occupied molecular orbit (HOMO) and lowest unoccupied molecular orbit (LUMO) energy levels through its redox potentials. The calculated energy of LUMO and HOMO levels were found to be −3.24 eV and −5.54 eV respectively, and the bandgap energy was calculated to be 2.30 eV. This finding shows best proximity with the calculated optical band energy value of 2.39 eV through the absorbance spectra of pure RuC dye in ethanol.

Fig. 7 illustrates the optical absorbance and Tauc plot for 0.3 mM RuC dye sensitized mesoporous TiO_2 electrode. RuC has strong absorption in the near UV region with a sharp decay tailing at around 516 nm. It was found that the calculated bandgap of RuC is 2.40 eV, and this value is in a good proximate with the optical energy band values of pure RuC in ethanol which is calculated viaλ_{onset} of absorbance spectrum as shown in Fig. 3**(b)**. Notably, the energy gap of RuC remains constant upon the thin film fabrication as for the pure RuC. This reveals that the process of RuC modification on mesoporous TiO_2 doesn't cause any changes in the structure of RuC dye.

Table 1 compares the MEC and wavelength corresponding to

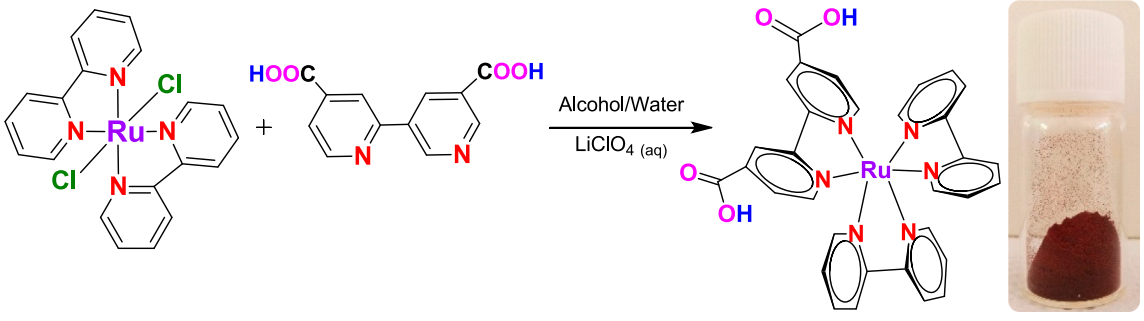

Fig. 2. The scheme represents the steps involved in the synthesis of RuC dye. An optical photograph represents the synthesized RuC dye.

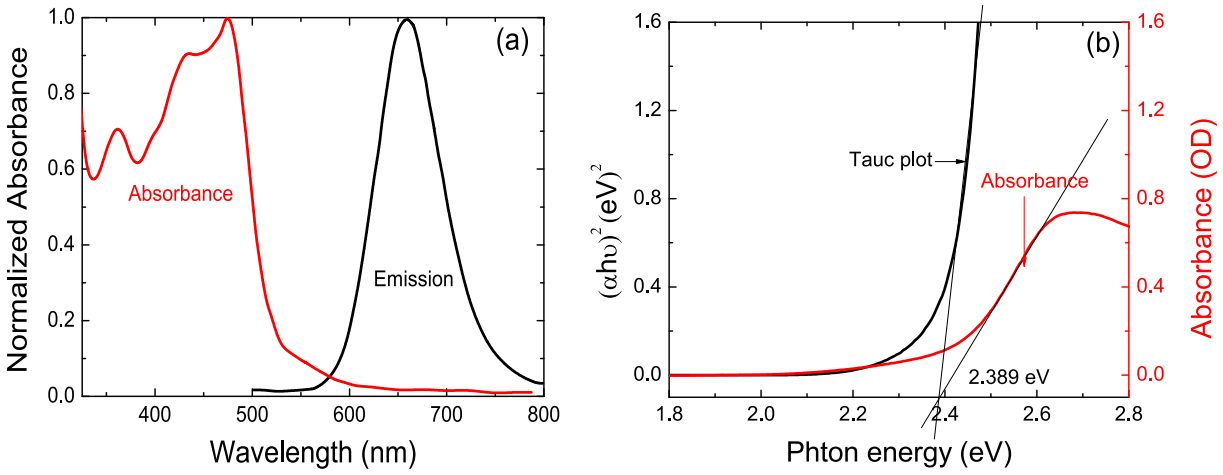

Fig. 3. **(a)** Absorbance and emission spectrum, and **(b)** Tauc plot of 0.05 mM RuC dye in ethanol.

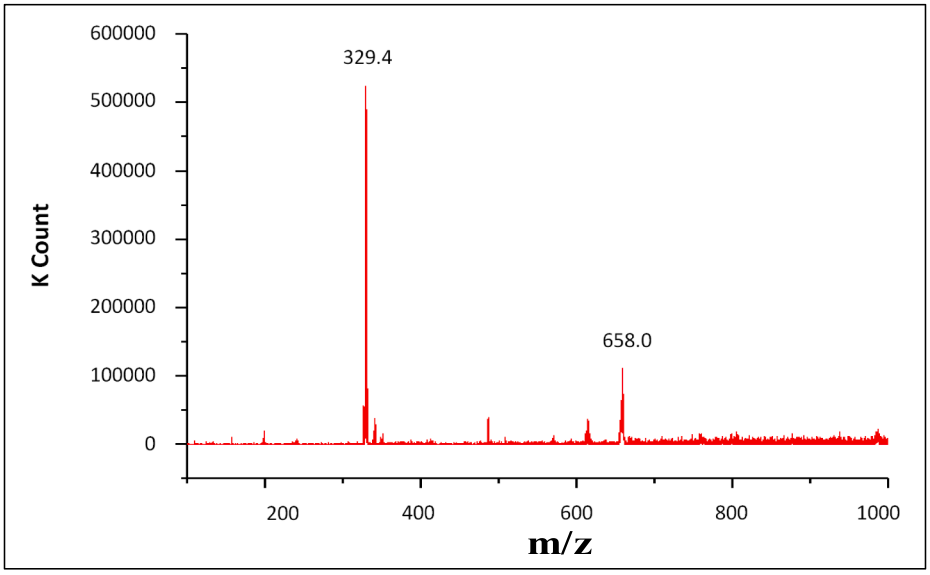

Fig. 4. Mass spectrum of RuC.

maximum absorption of the RuC dye with commercial Z907 (Yu et al., 2009), N3 and N719 (Arifin et al., 2018) dyes. The MEC of RuC was calculated from Fig. 3**. (b)** and, MEC of other dyes are directly taken from the corresponding literature and material safety data sheet. The MEC of RuC is higher compared to other three dyes, which shows that the carrier generation is higher in RuC and it has an absorption maxima at 463 nm. However, the absorption of TiO_2 is in UV region and therefore, the sensitization of RuC on TiO_2 surface can exhibit an extended absorption spectrum from near UV to visible region. Higher carrier generation and higher MEC make RuC an interesting dye for further analysis, for example on DSSCs.

3.2. Photovoltaic performance

As described in methods, the solid and liquid state dye sensitized solar cells were respectively fabricated with solid Spiro-OMeTAD electrolyte and liquid I^-/I^{3-} electrolyte as the hole transporting medium. First, the optical performance of synthetic RuC modified mesoporous nanocrystalline TiO_2 electrodes were analyzed with the presence of solid Spiro-OMeTAD electrolyte. Fig. 8 shows the normalized absorption spectra of TiO_2/RuC and TiO_2/RuC/Spiro-OMeTAD nanocomposites. It was noted that RuC having a strong absorption with an absorption peak at 463 nm near UV region. Further, the modification of Spiro-OMeTAD on top of the RuC enhances the overall absorbance of nanocomposite by expanding the spectral area under visible region, which is a crucial factor to enhance the carrier generation in DSSCs.

According to the energy levels shown in Fig. 9, the LUMO level of Spiro-OMeTAD and the Conduction Band (CB) of TiO_2 are relatively close to each other. The energy separation between the CB edge of TiO_2 and HOMO of Spiro-OMeTAD is nearly 1 eV. With the addition of RuC sensitizer, TiO_2/RuC/Spiro-OMeTAD/Au is the solid-state DSSC device structure and the separation between CB edge of TiO_2 and HOMO of donor RuC is around 1.4 eV. The separation between LUMO level of RuC and the HOMO level of Spiro-OMeTAD is around 1.9 eV which is higher compared to the Z907 and N719 sensitized structures. It is clear that the inter layering of RuC can reduce the electron recombination by increasing the separation between CB energy level of TiO_2 (electron transporter) and HOMO energy level of Spiro-OMeTAD (hole transporter) layers. Similar studies have already been reported with RuC interface modified hybrid TiO_2/P3HT solar cells, that the fabricated solar cells resulted in reduced recombination and improved carrier lifetime in the TiO_2/P3HT nanocomposite solar cells (Pirashanthan et al., 2020). The HOMO level of RuC respect to I^-/I^{3-} redox potential is in the position to fulfill proper regeneration of exited dye molecules.

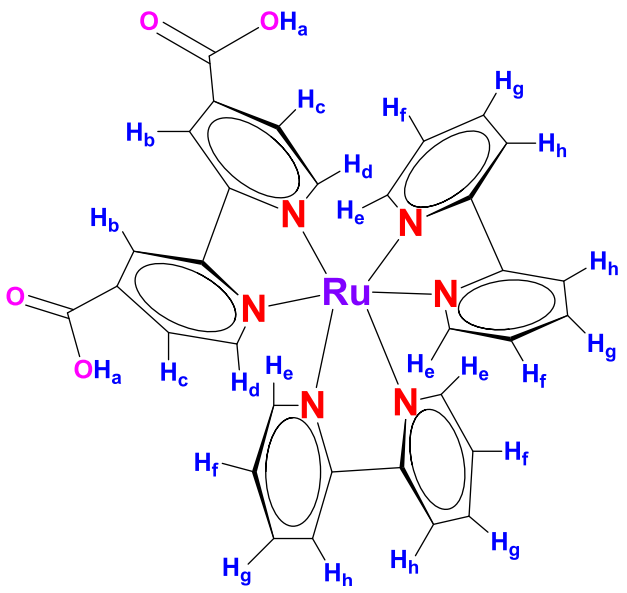

Fig. 5. Nuclear Magnetic Resonance Spectroscopic (NMR) interpretation of RuC dye.

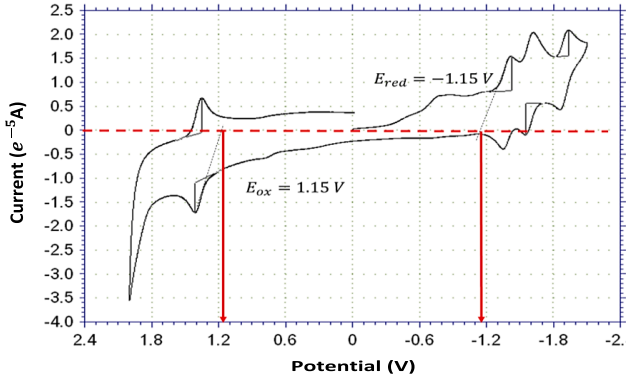

Fig. 6. Bandgap calculation by CV measurement.

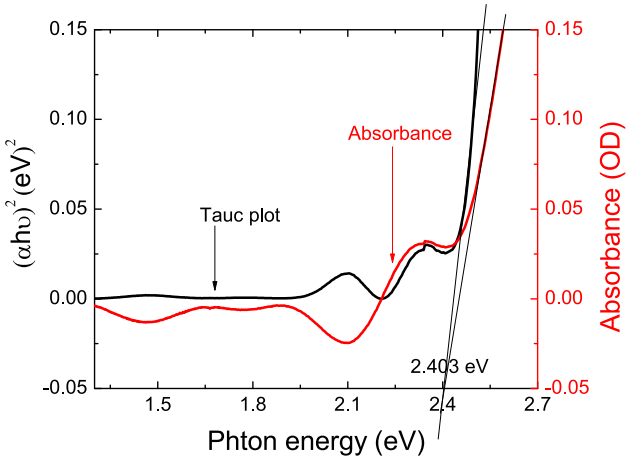

Fig. 7. Absorption and Tauc plot for RuC modified TiO_2 thin films for bandgap calculation.

Energy of LUMO level of RuC lies well above TiO_2 conduction band energy about 0.9 eV which is high compared to the LUMO levels of Z907 and N719 dyes with CB of TiO_2. That will enhance electron injection in carboxyl based ruthenium RuC sensitized DSSCs. The sensitizing of RuC dye of TiO_2 assist the electron transport from Spiro-OMeTAD in the reduction of the dye molecule to the ground state, thus it acts as a hole blocking layer.

Table 1
The molar extinction coefficient (MEC) and wavelength for maximum absorption of the Z907, N3, N719 and RuC dyes.

Dye	Molar Extinction Coefficient ($M^{-1}cm^{-1}$)	Wavelength corresponding to maximum absorption (nm)
Z907	12,200	521
N3	13,000	518
N719	14,100	515
RuC	14,746	463

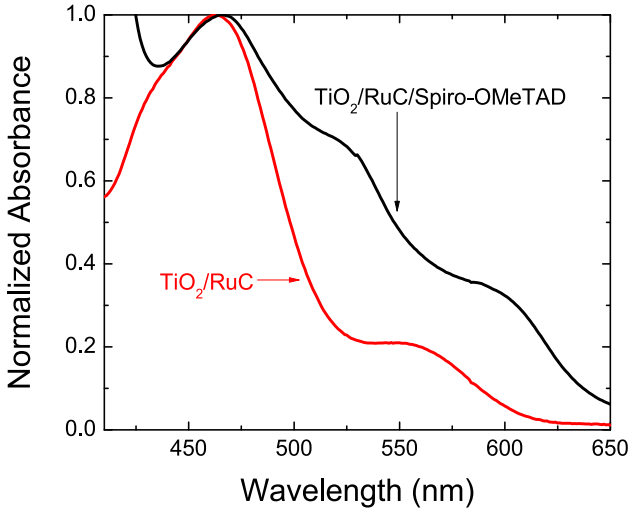

Fig. 8. Normalized absorbance spectra of TiO_2/RuC dye and TiO_2/RuC/Spiro-OMeTAD coated mesoporous TiO_2 electrodes.

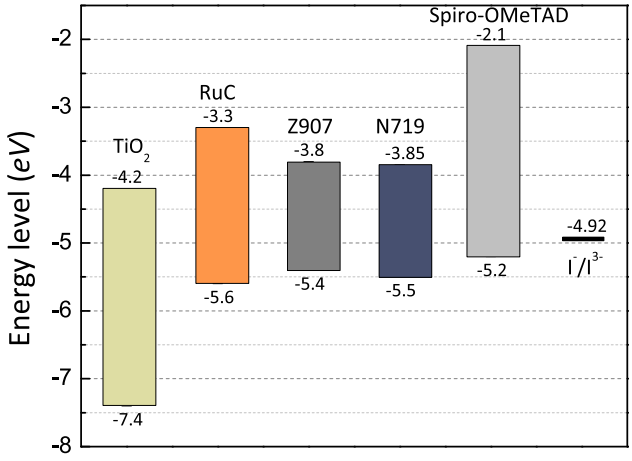

Fig. 9. Energy level diagram showing the HOMO and LUMO energy levels of each RuC, Z907 and N719 dyes, and their position relative to the energy levels of TiO_2 (Kajana et al., 2020; Pirashanthan et al., 2020, 2019), Spiro-OMeTAD (Wang et al., 2017) and I^-/I^{3-} (Cariello et al., 2016) redox potential. The energy levels for Z907 and N719 dyes were directly taken from the literature (Nosheen et al., 2016).

Fig. 10 **(a)** shows the J-V curves of the fabricated DSSCs with liquid and solid electrolytes. It can be seen that the RuC dye can efficiently produce photo generated carriers. The PCE of the device with liquid electrolyte is around 1.8% while the efficiency with solid-state

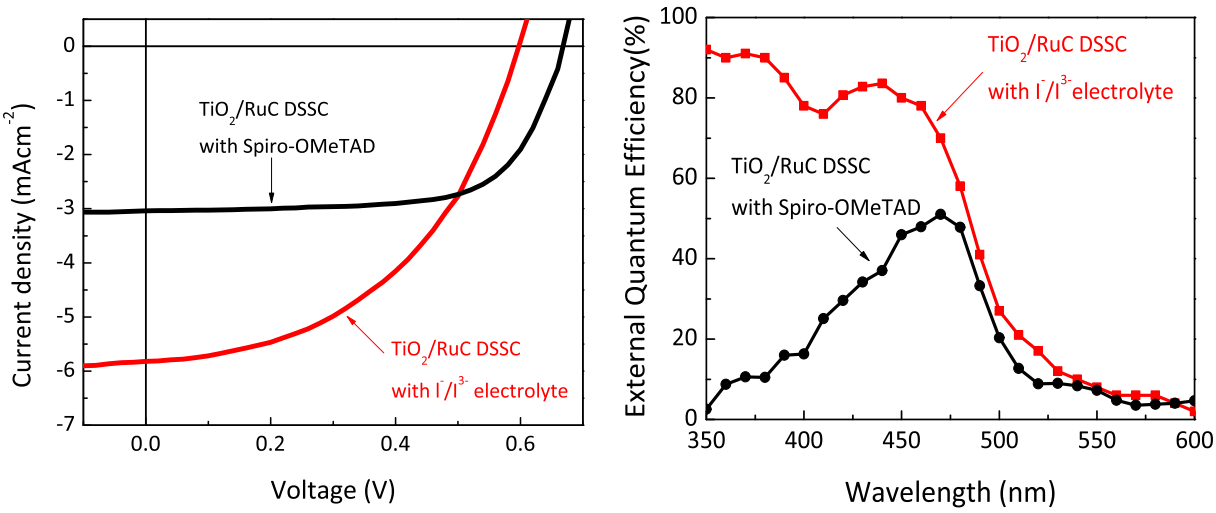

Fig. 10. **(a)** J-V curves of DSSCs with liquid I^-/I^{3-} and solid Spiro-OMeTAD as the hole transporting mediums and **(b)** EQE spectra of the DSSCs with liquid I^-/I^{3-} and spiro-OMeTAD hole transporting mediums.

electrolyte is around 1.2%. Lower J_{SC} of the solid-state device can be attributed to relatively higher hole transporting resistance of the Spiro-OMeTAD electrolyte compared to that of liquid I^-/I^{3-} electrolyte (Fabregat-Santiago et al., 2009). Fig. 10 **(b)** illustrates the EQE spectra of the DSSC with liquid and solid electrolyte. The EQE spectra covers the UV region with a plateau of more than 80% in the absorbance region of the RuC dye ensures that the dye is an excellent candidate for photon to electron conversion. Further, it was evidenced with the improved Jsc present with the liquid state DSSC. However, the EQE at UV region is lower when the Spiro-OMeTAD is used as the hole conductor. As discussed, the hole transporting resistance of the Spiro-OMeTAD compared to that of liquid electrolyte is much higher and this could limit the EQE of the cells at high energy UV-region. Moreover, both solid and liquid state DSSCs have shown to have high V_{OC} (>0.60 V) and fill factor (>0.52) for fabricated solar cells. The V_{OC} and fill factor are lower for the liquid-state compared to solid-state DSSCs as shown in Table 2. This is probably attributed to the compatibility of RuC dye with Spiro-OMeTAD hole transporter. In summary, the carrier generation of this novel, synthetic, cost-effective RuC dye and its narrow band gap make RuC to be used as a sensitizer in both solid and liquid state DSSCs.

4. Conclusions

In this study, a carboxylic acid-based ruthenium RuC dye was synthesized and its applicability towards Dye-Sensitized Solar Cells was verified by fabricating solid Spiro-OMeTAD electrolyte and liquid I^-/I^3 electrolyte based solar cells. The novel crystalline solid RuC dye that was synthesized had high purity and a yield percentage of 45%. Formation of $Ru(bpy)_2(dcbpy)(ClO_4)_2$[(bpy)2,2′-bipyridine;dcbpy = 4,4′-dicarboxy-2,2′-bipyridine] (RuC) was confirmed with Mass spectroscopy and NMR analysis. The calculated optical band gap of 2.30 eV via CV was also confirmed with the Tauc plots obtained for RuC modified thin films. The RuC dye employed as a sensitizer in Tatiana based solid and liquid state DSSCs. The dye showed significant photocurrent generation when it is deposited onto a TiO_2 nanoporous layer. The presence of RuC enhances both the J_{SC} and V_{OC}. The PCE of the solid and liquid electrolyte DSSCs was about 1.2% and 1.8%, respectively. The EQE plateau of more than 80% in the absorbance region of the dye ensures that the RuC is an excellent candidate for carrier generation in near UV region. Moreover, the well-matched energy level position of RuC dye shows high potential for efficient charge transfer in DSSCs. The carboxylic acid based synthetic RuC dye is, therefore, a promising material to enhance the performance of both solid and liquid state DSSCs. Further, the synthesis of RuC is very less costly compared to commercial ruthenium-based dyes.

Table 2
Device parameters for solid-state and liquid state DSSCs of champion devices.[a]

Type of DSSC	J_{SC} (mA/cm^2)	V_{OC} (V)	FF	PCE %
Solid-state	3.04	0.68	0.60	1.24
Liquid-state	5.82	0.60	0.52	1.82

[a] The DSSCs were tested under conditions of 1 sun illuminations.

The successful synthesis of low-cost and efficient sensitizers of this kind will lead to reduce the production cost of future DSSCs.

Declaration of Competing Interest

The authors declare that they have no known competing financial interests or personal relationships that could have appeared to influence the work reported in this paper.

Acknowledgements

All others acknowledge to Capacity Building and Establishment of Research Consortium (CBERC) (grant number LKA-3182-HRNCET) and, Higher Education and Research collaboration on Nanomaterials for Clean Energy Technologies (HRNCET) (grant number NORPART/2016/10237) projects for the research funding (http://project.jfn.ac.lk/hrncet/).

Appendix A. Supplementary material

Supplementary data to this article can be found online at https://doi.org/10.1016/j.solener.2021.07.056.

References

Abate, A., Planells, M., Hollman, D.J., Stranks, S.D., Petrozza, A., Kandada, A.R.S., Vaynzof, Y., Pathak, S.K., Robertson, N., Snaith, H.J., 2014. An organic "donor-free" dye with enhanced open-circuit voltage in solid-state sensitized solar cells. Adv. Energy Mater. https://doi.org/10.1002/aenm.201400166.

Abdellah, I.M., El-Shafei, A., 2020. Synthesis and characterization of novel tetra anchoring A2-D-D-D-A2 architecture sensitizers for efficient dye-sensitized solar cells. Sol. Energy 198, 25–35. https://doi.org/10.1016/j.solener.2020.01.040.

Abdellah, I.M., Koraiem, A.I., El-Shafei, A., 2019. Structure-property relationship of novel monosubstituted Ru (II) complexes for high photocurrent and high efficiency DSSCs: Influence of donor versus acceptor ancillary ligand on DSSCs performance. Sol. Energy 177, 642–651. https://doi.org/10.1016/j.solener.2018.11.047.

Aguirre-Araque, J.S., Guimaraes, R.R., Toma, H.E., 2020. Chemistry of ternary monocarboxyterpyridine-bipyridine-trimercaptotriazine ruthenium complexes and

application in dye sensitized solar cells. Polyhedron 182, 114513. https://doi.org/10.1016/j.poly.2020.114513.
Arifin, Z., Suyitno, S., Hadi, S., Sutanto, B., 2018. Improved Performance of Dye-Sensitized Solar Cells with TiO2 Nanoparticles/Zn-Doped TiO2 Hollow Fiber Photoanodes. Energies 11, 2922. https://doi.org/10.3390/en11112922.
Baktash, A., Khoshnevisan, B., Sasani, A., Mirabbaszadeh, K., 2016. Effects of carboxylic acid and phosphonic acid anchoring groups on the efficiency of dye sensitized solar cells: A computational study. Org. Electron. 33, 207–212. https://doi.org/10.1016/j.orgel.2016.03.013.
Braumüller, M., Schulz, M., Staniszewska, M., Sorsche, D., Wunderlin, M., Popp, J., Guthmuller, J., Dietzek, B., Rau, S., 2016. Synthesis and characterization of ruthenium and rhenium dyes with phosphonate anchoring groups. Dalt. Trans. 45, 9216–9228. https://doi.org/10.1039/c6dt01047d.
Cariello, M., Ahn, S., Park, K.W., Chang, S.K., Hong, J., Cooke, G., 2016. An investigation of the role increasing π-conjugation has on the efficiency of dye-sensitized solar cells fabricated from ferrocene-based dyes. RSC Adv. 6, 9132–9138. https://doi.org/10.1039/c5ra21565j.
Chang, W.C., Lee, C.H., Yu, W.C., Lin, C.M., 2012. Optimization of dye adsorption time and film thickness for efficient ZnO dye-sensitized solar cells with high at-rest stability. Nanoscale Res. Lett. 7, 1–10. https://doi.org/10.1186/1556-276X-7-688.
Chen, J., Peng, T., Fan, K., Xia, J., 2011. Iodine-free quasi solid-state dye-sensitized solar cells based on ionic liquid and alkali salt. J. Mater. Chem. 21, 16448. https://doi.org/10.1039/c1jm12710a.
Deiana, C., Fois, E., Martra, G., Narbey, S., Pellegrino, F., Tabacchi, G., 2016. On the Simple Complexity of Carbon Monoxide on Oxide Surfaces: Facet-Specific Donation and Backdonation Effects Revealed on TiO2 Anatase Nanoparticles. ChemPhysChem 1956–1960. https://doi.org/10.1002/cphc.201600284.
Deiana, C., Tabacchi, G., Maurino, V., Coluccia, S., Martra, G., Fois, E., 2013. Surface features of TiO2 nanoparticles: Combination modes of adsorbed CO probe the stepping of (101) facets. Phys. Chem. Chem. Phys. 15, 13391–13399. https://doi.org/10.1039/c3cp51524a.
Dissanayake, M.A.K.L., Jaseetharan, T., Senadeera, G.K.R., Kumari, J.M.K.W., Thotawatthage, C.A., Mellander, B.E., Albinson, I., Furlani, M., 2019. Highly efficient, PbS: Hg quantum dot–sensitized, plasmonic solar cells with TiO2 triple-layer photoanode. J. Solid State Electrochem. 23, 1787–1794. https://doi.org/10.1007/s10008-019-04280-y.
Dissanayake, M.A.K.L., Jaseetharan, T., Senadeera, G.K.R., Mellander, B.-E., Albinsson, I., Furlani, M., Kumari, J.M.K.W., 2021. Solid-state solar cells co-sensitized with PbS/CdS quantum dots and N719 dye and based on solid polymer electrolyte with binary cations and nanofillers. J. Photochem. Photobiol. A Chem. 405, 112915 https://doi.org/10.1016/j.jphotochem.2020.112915.
El Bitar Nehme, V.A., El Bitar Nehme, M.A., Ghaddar, T.H., 2019. New pyridyl-based dyes for co-sensitization in dye sensitized solar cells. Sol. Energy 187, 108–114. https://doi.org/10.1016/j.solener.2019.05.037.
Fabregat-Santiago, F., Bisquert, J., Cevey, L., Chen, P., Wang, M., Zakeeruddin, S.M., Grätzel, M., 2009. Electron transport and recombination in solid-state dye solar cell with spiro-OMeTAD as hole conductor. J. Am. Chem. Soc. 131, 558–562. https://doi.org/10.1021/ja805850q.
Fournier, M., Hoogeveen, D.A., Bonke, S.A., Spiccia, L., Simonov, A.N., 2018. Cooperative silanetriolate-carboxylate sensitiser anchoring for outstanding stability and improved performance of dye-sensitised photoelectrodes. Sustain. Energy Fuels 2, 1707–1718. https://doi.org/10.1039/c8se00056e.
Giribabu, L., Singh, V.K., Vijay Kumar, C., Soujanya, Y., Gopal Reddy, V., Yella Reddy, P., 2011. Organic-ruthenium(II) polypyridyl complex based sensitizer for dye-sensitized solar cell applications. Adv. Optoelectron. 2011 https://doi.org/10.1155/2011/294353.
Gorduk, S., Altindal, A., 2019. Peripherally tetra-substituted metallophthalocyanines bearing carboxylic acid groups for efficient dye sensitized solar cells. J. Mol. Struct. 1196, 747–753. https://doi.org/10.1016/j.molstruc.2019.07.027.
Kajana, T., Velauthapillai, D., Shivatharsiny, Y., Ravirajan, P., Yuvapragasam, A., Senthilnanthanan, M., 2020. Structural and photoelectrochemical characterization of heterostructured carbon sheet/Ag2MoO4-SnS/Pt photocapacitor. J. Photochem. Photobiol. A Chem. 401, 112784 https://doi.org/10.1016/j.jphotochem.2020.112784.
Karakuş, M.Ö., Yakışıklıer, M.E., Delibaş, A., Ayyıldız, E., Çetin, H., 2020. Anionic and cationic polymer-based quasi-solid-state dye-sensitized solar cell with poly(aniline) counter electrode. Sol. Energy 195, 565–572. https://doi.org/10.1016/j.solener.2019.11.088.
Khan, M.Z.H., Al-Mamun, M.R., Halder, P.K., Aziz, M.A., 2017. Performance improvement of modified dye-sensitized solar cells. Renew. Sustain. Energy Rev. 71, 602–617. https://doi.org/10.1016/j.rser.2016.12.087.
Lee, C.-P., Ho, K.-C., 2018. Poly(ionic liquid)s for dye-sensitized solar cells: A mini-review. Eur. Polym. J. 108, 420–428. https://doi.org/10.1016/j.eurpolymj.2018.09.022.
Lee, C.-P., Li, C.-T., Ho, K.-C., 2017. Use of organic materials in dye-sensitized solar cells. Mater. Today 20, 267–283. https://doi.org/10.1016/j.mattod.2017.01.012.
Louazri, L., Amine, A., Bouzzine, S.M., Hamidi, M., Bouachrine, M., 2016. Photovoltaic properties of Zn-Complexed-phtalocyanine and derivatives for DSSCs application. J. Mater. Environ. Sci. 7, 2305–2313.
Mahoney, L., Rasalingam, S., Wu, C., Koodali, R.T., 2015a. Nanocasting of Periodic Mesoporous Materials as an Effective Strategy to Prepare Mixed Phases of Titania 21881–21895. https://doi.org/10.3390/molecules201219812.
Mahoney, L., Rasalingam, S., Wu, C., Peng, R., Koodali, R.T., 2015b. Aging dependent phase transformation of mesostructured titanium dioxide nanomaterials prepared by evaporation-induced self-assembly process : Implications for solar hydrogen production 2, 230–242. https://doi.org/10.3934/matersci.2015.230.
Maleki, E., Ranjbar, M., Kahani, S.A., 2021. The Effect of Antisolvent Dropping Delay Time on the Morphology and Structure of the Perovskite Layer in the Hole Transport Material Free Perovskite Solar Cells. Prog. Color. Color. Coatings 14, 47–54. https://doi.org/10.30509/pccc.2021.81671.
Mariotti, N., Bonomo, M., Fagiolari, L., Barbero, N., Gerbaldi, C., Bella, F., Barolo, C., 2020. Recent advances in eco-friendly and cost-effective materials towards sustainable dye-sensitized solar cells. Green Chem. 22, 7168–7218. https://doi.org/10.1039/D0GC01148G.
Mehmood, U., Al-Ahmed, A., Al-Sulaiman, F.A., Malik, M.I., Shehzad, F., Khan, A.U.H., 2017. Effect of temperature on the photovoltaic performance and stability of solid-state dye-sensitized solar cells: A review. Renew. Sustain. Energy Rev. 79, 946–959. https://doi.org/10.1016/j.rser.2017.05.114.
Neuthe, K., Bittner, F., Stiemke, F., Ziem, B., Du, J., Zellner, M., Wark, M., Schubert, T., Haag, R., 2014. Phosphonic acid anchored ruthenium complexes for ZnO-based dye-sensitized solar cells. Dye. Pigment. 104, 24–33. https://doi.org/10.1016/j.dyepig.2013.12.018.
Nosheen, E., Shah, S.M., Hussain, H., Murtaza, G., 2016. Photo-sensitization of ZnS nanoparticles with renowned ruthenium dyes N3, N719 and Z907 for application in solid state dye sensitized solar cells: A comparative study. J. Photochem. Photobiol. B Biol. 162, 583–591. https://doi.org/10.1016/j.jphotobiol.2016.07.033.
O'Regan, B., Grätzel, M., 1991. A low-cost, high-efficiency solar cell based on dye-sensitized colloidal TiO2 films. Nature 353, 737–740. https://doi.org/10.1038/353737a0.
Oh, J., Ghann, W., Kang, H., Nesbitt, F., Providence, S., Uddin, J., 2018. Comparison of the performance of dye sensitized solar cells fabricated with ruthenium based dye sensitizers: Di-tetrabutylammonium cis-bis(isothiocyanato)bis(2,2′-bipyridyl-4,4′-dicarboxylato)ruthenium(II) (N719) and tris(bipyridine)ruthenium(II) chloride. Inorganica Chim. Acta 482, 943–950. https://doi.org/10.1016/j.ica.2018.07.019.
Omar, A., Ali, M.S., Abd Rahim, N., 2020. Electron transport properties analysis of titanium dioxide dye-sensitized solar cells (TiO2-DSSCs) based natural dyes using electrochemical impedance spectroscopy concept: A review. Sol. Energy 207, 1088–1121. https://doi.org/10.1016/j.solener.2020.07.028.
Park, H., Bae, E., Lee, J.J., Park, J., Choi, W., 2006. Effect of the anchoring group in ru-bipyridyl sensitizers on the photoelectrochemical behavior of dye-sensitized TiO2 electrodes: Carboxylate versus phosphonate linkages. J. Phys. Chem. B 110, 8740–8749. https://doi.org/10.1021/jp060397e.
Patrocinio, A.O.T., Schneider, J., França, M.D., Santos, L.M., Caixeta, B.P., Machado, A.E. H., Bahnemann, D.W., 2015. Charge carrier dynamics and photocatalytic behavior of TiO2 nanopowders submitted to hydrothermal or conventional heat treatment. RSC Adv. 5, 70536–70545. https://doi.org/10.1039/c5ra13291f.
Pirashanthan, A., Murugathas, T., Mariappan, K., Ravirajan, P., Velauthapillai, D., Yohi, S., 2020. A multifunctional ruthenium based dye for hybrid nanocrystalline titanium dioxide/poly(3-hexylthiophene) solar cells. Mater. Lett. 274, 127997 https://doi.org/10.1016/j.matlet.2020.127997.
Pirashanthan, A., Murugathas, T., Robertson, N., Ravirajan, P., Velauthapillai, D., 2019. A Quarterthiophene-Based Dye as an Efficient Interface Modifier for Hybrid Titanium Dioxide/Poly(3-hexylthiophene)(P3HT) Solar Cells. Polymers (Basel). 11, 1752. https://doi.org/10.3390/polym11111752.
Prashanthan, K., Thivakarasarma, T., Ravirajan, P., Planells, M., Robertson, N., Nelson, J., 2017. Enhancement of hole mobility in hybrid titanium dioxide/poly(3-hexylthiophene) nanocomposites by employing an oligothiophene dye as an interface modifier. J. Mater. Chem. C 5, 11758–11762. https://doi.org/10.1039/c7tc02225e.
Rasalingam, S., Peng, R., Koodali, R.T., 2015a. An insight into the adsorption and photocatalytic degradation of rhodamine B in periodic mesoporous materials. Appl. Catal. B Environ. 174–175, 49–59. https://doi.org/10.1016/j.apcatb.2015.02.040.
Rasalingam, S., Peng, R., Wu, C.M., Mariappan, K., Koodali, R.T., 2015b. Robust and effective Ru-bipyridyl dye sensitized Ti-MCM-48 cubic mesoporous materials for photocatalytic hydrogen evolution under visible light illumination. Catal. Commun. 65, 14–19. https://doi.org/10.1016/j.catcom.2015.02.019.
Ravirajan, P., Atienzar, P., Nelson, J., 2012. Post-Processing Treatments in Hybrid Polymer/Titanium Dioxide Multilayer Solar Cells. J. Nanoelectron. Optoelectron. 7, 498–502. https://doi.org/10.1166/jno.2012.1379.
Senthilnanthan, M., Ho, D.P., Vigneswaran, S., Ngo, H.H., Shon, H.K., 2010. Visible light responsive ruthenium-doped titanium dioxide for the removal of metsulfuron-methyl herbcide in aqueous phase. Sep. Purif. Technol. 75, 415–419. https://doi.org/10.1016/j.seppur.2010.05.019.
Shanmugaratnam, S., Velauthapillai, D., Ravirajan, P., Christy, A.A., Shivatharsiny, Y., 2019. CoS2/TiO2 nanocomposites for hydrogen production under UV irradiation. Materials (Basel). 12, 1–9. https://doi.org/10.3390/MA12233882.
Sodeyama, K., Sumita, M., ORourke, C., Terranova, U., Islam, A., Han, L., Bowler, D.R., Tateyama, Y., 2012. Protonated carboxyl anchor for stable adsorption of Ru N749 dye (black dye) on a TiO 2 anatase (101) surface. J. Phys. Chem. Lett. 3, 472–477. https://doi.org/10.1021/jz201583n.
Song, H.K., Park, Y.H., Han, C.H., Jee, J.G., 2009. Synthesis of ruthenium complex and its application in dye-sensitized solar cells. J. Ind. Eng. Chem. 15, 62–65. https://doi.org/10.1016/j.jiec.2008.08.011.
Sugathan, V., John, E., Sudhakar, K., 2015. Recent improvements in dye sensitized solar cells: A review. Renew. Sustain. Energy Rev. 52, 54–64. https://doi.org/10.1016/j.rser.2015.07.076.
Swarnalatha, K., Kamalesu, S., Subramanian, R., 2016. Mono and binuclear ruthenium (II) complexes containing 5-chlorothiophene-2-carboxylic acid ligands: Spectroscopic analysis and computational studies. J. Mol. Struct. 1123, 416–425. https://doi.org/10.1016/j.molstruc.2016.07.048.

Tabacchi, G., Fabbiani, M., Mino, L., Martra, G., Fois, E., 2019. The Case of Formic Acid on Anatase TiO2(101): Where is the Acid Proton? Angew. Chemie - Int. Ed. 58, 12431–12434. https://doi.org/10.1002/anie.201906709.

Tsaturyan, A., Machida, Y., Akitsu, T., Gozhikova, I., Shcherbakov, I., 2018. Binaphthyl-containing Schiff base complexes with carboxyl groups for dye sensitized solar cell: An experimental and theoretical study. J. Mol. Struct. 1162, 54–62. https://doi.org/10.1016/j.molstruc.2018.02.082.

Veronese, L., Quartapelle Procopio, E., Moehl, T., Panigati, M., Nonomura, K., Hagfeldt, A., 2019. Triarylamine-based hydrido-carboxylate rhenium(i) complexes as photosensitizers for dye-sensitized solar cells. Phys. Chem. Chem. Phys. 21, 7534–7543. https://doi.org/10.1039/c9cp00856j.

Wang, X., Deng, L.L., Wang, L.Y., Dai, S.M., Xing, Z., Zhan, X.X., Lu, X.Z., Xie, S.Y., Huang, R. Bin, Zheng, L.S., 2017. Cerium oxide standing out as an electron transport layer for efficient and stable perovskite solar cells processed at low temperature. J. Mater. Chem. A 5, 1706–1712. https://doi.org/10.1039/c6ta07541j.

Wu, J., Lan, Z., Lin, J., Huang, M., Huang, Y., Fan, L., Luo, G., 2015. Electrolytes in Dye-Sensitized Solar Cells. Chem. Rev. 115, 2136–2173. https://doi.org/10.1021/cr400675m.

Wu, J., Lan, Z., Lin, J., Huang, M., Huang, Y., Fan, L., Luo, G., Lin, Y., Xie, Y., Wei, Y., 2017. Counter electrodes in dye-sensitized solar cells. Chem. Soc. Rev. 46, 5975–6023. https://doi.org/10.1039/c6cs00752j.

Yu, Q., Liu, S., Zhang, M., Cai, N., Wang, Y., Wang, P., 2009. An Extremely High Molar Extinction Coefficient Ruthenium Sensitizer in Dye-Sensitized Solar Cells: The Effects of π-Conjugation Extension. J. Phys. Chem. C 113, 14559–14566. https://doi.org/10.1021/jp904096g.

Zhang, J., Freitag, M., Hagfeldt, A., Boschloo, G., 2018. Solid-State Dye-Sensitized Solar Cells, in: Tian, H., Boschloo, G., Hagfeldt, A. (Eds.), Molecular Devices for Solar Energy Conversion and Storage. Springer Singapore, Singapore, pp. 151–185. https://doi.org/10.1007/978-981-10-5924-7_4.